Radioluminescent nanophosphors enable multiplexed small-animal imaging

Colin M Carpenter,[1] Conroy Sun,[1] Guillem Pratx,[1] Hongguang Liu,[2] Zhen Cheng,[2] and Lei Xing[1,*]

[1]*Department of Radiation Oncology, School of Medicine, Stanford University, Stanford, CA USA 94305 USA*
[2]*Molecular Imaging Program at Stanford (MIPS), Department of Radiology and Bio-X Program, Canary Center at Stanford for Cancer Early Detection, Stanford University, California, 94305-5344 USA*
[*]*lei@stanford.edu*

Abstract: We demonstrate the ability to image multiple nanoparticle-based contrast agents simultaneously using a nanophosphor platform excited by either radiopharmaceutical or X-ray irradiation. These radioluminescent nanoparticles emit optical light at unique wavelengths depending on their lanthanide dopant, enabling multiplexed imaging. This study demonstrates the separation of two distinct nanophosphor contrast agents in gelatin phantoms with a recovered phosphor separation correlation of –0.98. The ability to distinguish the two nanophosphors and a Cerenkov component is then demonstrated in a small animal phantom. Combined with the high-resolution potential of low-scattering X-ray excitation, this imaging technique may be a promising method to probe molecular processes in living organisms.

OCIS codes: (110.4234) Multispectral and hyperspectral imaging; (170.0170) Medical optics and biotechnology; (160.4236) Nanomaterials.

References and links

1. M. Stroh, J. P. Zimmer, D. G. Duda, T. S. Levchenko, K. S. Cohen, E. B. Brown, D. T. Scadden, V. P. Torchilin, M. G. Bawendi, D. Fukumura, and R. K. Jain, "Quantum dots spectrally distinguish multiple species within the tumor milieu in vivo," Nat. Med. **11**(6), 678–682 (2005).
2. X. Wu, H. Liu, J. Liu, K. N. Haley, J. A. Treadway, J. P. Larson, N. Ge, F. Peale, and M. P. Bruchez, "Immunofluorescent labeling of cancer marker Her2 and other cellular targets with semiconductor quantum dots," Nat. Biotechnol. **21**(1), 41–46 (2003).
3. W. Cai, D.-W. Shin, K. Chen, O. Gheysens, Q. Cao, S. X. Wang, S. S. Gambhir, and X. Chen, "Peptide-labeled near-infrared quantum dots for imaging tumor vasculature in living subjects," Nano Lett. **6**(4), 669–676 (2006).
4. F. G. Blankenberg, "In vivo detection of apoptosis," J. Nucl. Med. **49**(Suppl 2), 81S–95S (2008).
5. X. Gao, W. C. W. Chan, and S. Nie, "Quantum-dot nanocrystals for ultrasensitive biological labeling and multicolor optical encoding," J. Biomed. Opt. **7**(4), 532–537 (2002).
6. I. L. Medintz, H. T. Uyeda, E. R. Goldman, and H. Mattoussi, "Quantum dot bioconjugates for imaging, labelling and sensing," Nat. Mater. **4**(6), 435–446 (2005).
7. A. P. Alivisatos, W. Gu, and C. Larabell, "Quantum dots as cellular probes," Annu. Rev. Biomed. Eng. **7**(1), 55–76 (2005).
8. C. Sun, C. Carpenter, G. Pratx, and L. Xing, "Facile Synthesis of Amine-Functionalized Eu^{3+}-Doped $La(OH)_3$ Nanophosphors for Bioimaging," Nanoscale Res. Lett. **6**(24), (2011).
9. H. Chander, "Development of nanophosphors - A review," Mater. Sci. Eng. Rep. **49**(5), 113–155 (2005).
10. J. Shen, L.-D. Sun, and C.-H. Yan, "Luminescent rare earth nanomaterials for bioprobe applications," Dalton Trans. **24**(42), 5687–5697 (2008).
11. C. M. Carpenter, C. Sun, G. Pratx, R. Rao, and L. Xing, "Hybrid x-ray/optical luminescence imaging: characterization of experimental conditions," Med. Phys. **37**(8), 4011–4018 (2010).
12. G. Pratx, C. M. Carpenter, C. Sun, and L. Xing, "X-ray luminescence computed tomography via selective excitation: a feasibility study," IEEE Trans. Med. Imaging **29**(12), 1992–1999 (2010).
13. C. Sun, G. Pratx, C. M. Carpenter, H. Liu, Z. Cheng, S. S. Gambhir, and L. Xing, "Synthesis and radioluminescence of PEGylated Eu(3+) -doped nanophosphors as bioimaging probes," Adv. Mater. (Deerfield Beach Fla.) **23**(24), H195–H199 (2011).
14. H. Liu, X. Zhang, B. Xing, P. Han, S. S. Gambhir, and Z. Cheng, "Radiation-luminescence-excited quantum dots for in vivo multiplexed optical imaging," Small **6**(10), 1087–1091 (2010).

#162598 - $15.00 USD Received 7 Feb 2012; revised 6 Apr 2012; accepted 7 Apr 2012; published 7 May 2012

15. R. S. Dothager, R. J. Goiffon, E. Jackson, S. Harpstrite, and D. Piwnica-Worms, "Cerenkov radiation energy transfer (CRET) imaging: a novel method for optical imaging of PET isotopes in biological systems," PLoS ONE **5**(10), e13300 (2010).
16. M. A. Lewis, V. D. Kodibagkar, O. K. Öz, and R. P. Mason, "On the potential for molecular imaging with Cerenkov luminescence," Opt. Lett. **35**(23), 3889–3891 (2010).
17. J. Axelsson, S. C. Davis, D. J. Gladstone, and B. W. Pogue, "Cerenkov emission induced by external beam radiation stimulates molecular fluorescence," Med. Phys. **38**(7), 4127–4132 (2011).

1. Introduction

The application of luminescent nanoparticles, such as quantum dots, in diagnostic molecular imaging is receiving much attention due to the potential to improve the differentiation between normal and malignant tissue by identifying signatures of disease [1]. For example, multicolored quantum dots enable the ability to probe multiple signatures of disease simultaneously; this is recognized to be potentially more beneficial than visualizing a single species [2]. Examples of these molecular markers include the $\alpha_v\beta_3$ integrin and VEGF receptors as indicators for vascular angiogenesis [3], and the translocation of phosphatidylserine for apoptosis [4]. The advantage of nanoparticles in this context is that they may be tuned to emit at varying wavelengths, without severely altering their physical structure [5]. Although quantum dots have been investigated extensively for biological applications [6, 7], nanophosphors have been relatively ignored. Like quantum dots, nanophosphors have high quantum efficiencies, sharp emission peaks, high photostability, and emission wavelength tunability [8, 9]. Nanophosphors have a distinct advantage in that they may emit light when irradiated by ionizing radiation, a process called radioluminescence. This work demonstrates the multiplexing potential of these nanophosphors, using an exemplary nanophosphor system.

While radioluminescence of phosphor material has long been used in radiation detectors, the use of radioluminescent nanophosphors (RLNPs) in biological contexts is just beginning to be explored [10]. Novel applications currently under investigation for radioluminescent imaging (RLI) include direct biological feedback of molecular changes and tumor burden during radiation treatment. This information may be used as a means to enhance radiation treatment efficacy. In addition, RLI may be used to probe molecular information at a superior resolution to other molecular imaging modalities, such as Fluorescence Molecular Tomography (FMT), Positron Emission Tomography (PET), and Single Photon Computed Emission Tomography (SPECT), by collimating the excitation X-ray beam. This high-resolution technique, called X-ray Luminescence (Computed) Tomography (XLCT), utilizes narrowly-collimated X-ray beams to resolve deep-seated RLNPs. This is made possible because of the very low X-ray scatter in small-animals [11, 12].

This study demonstrates the potential use of RLNPs doped with different rare-earth luminescent centers to enable multiplexed RLI after excitation by ionizing radiation. In particular, it demonstrates the ability to recover the concentrations of each RLNP from multispectral images of the subject. To highlight the flexibility of this technique, multiplexed imaging was demonstrated using two different excitation schemes: radiopharmaceuticals (^{18}F) and X-ray radiation.

2. Methods

2.1 Imaging hardware

A custom imaging system was built to image and measure the concentrations of the nanophosphor contrast agents. A 512x512 pixel back-illuminated deep-cooled (–70C) CCD camera (ProEM, Princeton Instruments, Trenton, NJ) was outfitted with a F/#0.95 imaging lens (DO-5095, Navitar, Rochester, NY), and leaded glass was placed above the subject. Optical bandpass filters (546nm +/– 10nm for Tb^{3+} doped RLNPs, 700nm +/– 20nm for Eu^{3+} doped RLNPs; Andover Corporation, Salem, NH) were placed in front of the camera lens to

#162598 - $15.00 USD Received 7 Feb 2012; revised 6 Apr 2012; accepted 7 Apr 2012; published 7 May 2012

selectively collect emitted light in the unique spectral regions. A motorized platform adjusted the working distance of the camera to the subject and controlled the field of view. This imaging box was placed in the path of a superficial X-ray unit (Pantax Therapax, East Haven, CT), with voltage and current set to the X-ray tube 90keV and 10mA. This system was operated remotely from the control room of the X-ray unit, outside the X-ray room [11].

Optical spectra from the RLNPs (Fig. 1(a) and Fig. 1(b)) was collected by measuring the emission of dry powder samples in cuvettes. The distal end of a 10m 400µm optical fiber was placed in contact with the side of cuvettes containing each sample, while the proximal end was attached to a spectrophotometer (SP2150, Princeton Instruments) connected to the CCD camera, which was operated from the X-ray control room. Optical emission spectra within the visible and NIR range was acquired with custom software written in Labview (National Instruments, Austin, TX). By acquiring vertical spectral bins for each wavelength, image processing was used to remove X-ray noise, which stochastically appeared in the CCD. Alternatively, Cerenkov spectra was recorded by fitting a quadratic curve to data collected from a commercial imaging system (IVIS Spectrum, Perkin Elmer, Waltham, MA). The signal emitted from the radiopharmaceuticals was verified via a small animal Positron Emission Tomography (PET) system (Siemens R4 Micro-PET, Malvern, PA).

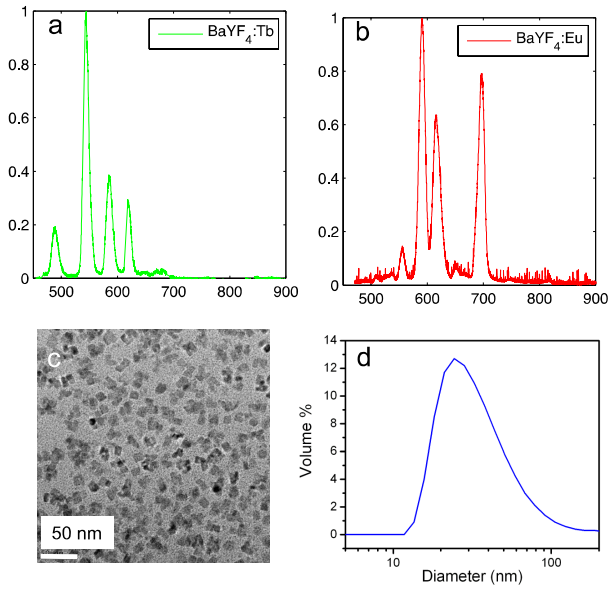

Fig. 1. (a) Radioluminecent spectrum of the $Ba_{0.55}Y_{0.3}F_2$:Tb^{3+} particles, which emit primarily in the green. (b) Radioluminecent spectrum of the $Ba_{0.55}Y_{0.3}F_2$:Eu^{3+} particles, which emit primarily in the red and near-infrared. (c) Transmission electron microscopy image of the RLNPs. (d) Hydrodynamic size distribution of the RLNPs as determined by dynamic light scattering.

2.2 Contrast agent synthesis

In this study, we demonstrate two possible dopants, europium (Eu^{3+}) and terbium (Tb^{3+}). A detailed description of the synthesis of these particles was recently described by Sun et al. [13]. The host barium yttrium fluoride ($Ba_{0.55}Y_{0.3}F_2$) nanocrystals were doped with either terbium (0.5%) or europium (0.5%) to produce emission maxima at 541nm and 586nm, respectively. Both RLNPs emitted additional spectral peaks towards the near infrared (NIR) at 629nm and 692nm, respectively, as seen from Fig. 1(a) and Fig. 1(b); these emission wavelengths enable imaging of deeper structures. The unique signatures emitted by each phosphor enabled the ability to perform multiplexing. The surfaces of the RLNPs were

#162598 - $15.00 USD Received 7 Feb 2012; revised 6 Apr 2012; accepted 7 Apr 2012; published 7 May 2012

modified with poly(ethylene glycol) (PEG, MW 600) through a ligand exchange process to achieve colloidal stability in aqueous solutions. These phosphors can be functionalized with a biotin linker bound to the PEG. Shown in Fig. 1(c) is the transmission electron microscopy (TEM) image of this RLNP platform with a cubic morphology and mean particle size of 14nm. The hydrodynamic size was determined by dynamic light scattering (DLS); particles with hydrodynamic size of ~27nm were the most common, as shown in Fig. 1(d).

2.3 Image multiplexing

To form images of the concentrations, c, of each of these particles, the light emitted, ϕ, was recorded over the several optical spectral regions defined by filter f_1 and filter f_2 to form images of the subject, $i_1 = \phi(f_1)$ and $i_2 = \phi(f_1)$. These images, and the pre-recorded reference spectra, ε, for $Ba_{0.55}Y_{0.3}F_2:Tb^{3+}$, ($\varepsilon_{Tb}$), $Ba_{0.55}Y_{0.3}F_2:Eu^{3+}$, ($\varepsilon_{Eu}$), and the Cerenkov luminescence, (ε_{Ch}), were input into a linear-least squares algorithm to extract the contributions from each nanophosphor. Reference spectra was collected with a calibrated spectrometer, thus enabling a quantitative comparison between the nanophosphors. Since Cerenkov light was generated from the F-18 radiotracer, it was necessary to account for the Cerenkov component for the experiments involving radiotracer excitation. For experiments involving X-ray excitation, the Cerenkov component was not present, since Cerenkov light arises from photons emitted from highly-energetic charged particles that are greater than the energy of charged particles created during X-ray excitation.

2.4 Experimental demonstration

To validate the ability of this method to image multiple nanophosphors simultaneously, five phantoms (99% DI water, 1% agarose) were fabricated containing Tb^{3+} and Eu^{3+} doped RLNPs of linearly varying concentrations (in units of mg/ml) and mixed in the following ratios: (0:10; 2.5:7.5; 5:5; 7.5:2.5; and 10:0). To demonstrate this method in a pre-clinical mouse model, four batches of RLNPs were each mixed with 52 μCi (Curie) of activity of 18-F and Matrigel (BD Biosciences, Sparks, MD) and injected into both forelegs and flanks of a nude mouse, with Eu^{3+}-doped RLNPs (Eu) only on the left foreleg, Tb^{3+}-doped RLNPs (Tb) only on the left flank, an equal mixture of Eu^{3+}-doped RLNPs and Tb^{3+}-doped RLNPs (Mix) on the right flank, and an inactive undoped nanophosphor control (Ctrl) on the right foreleg. For the radioisotope-excited experiment, the subject was imaged immediately after injection. For the X-ray-excited experiment several days later (after the 18-F had fully decayed), the same subject was placed in the imaging apparatus and excited by a 90keV X-ray source, which was transmitted through the dark-box. The same subject was imaged with the X-ray and radiopharmaceutical excitation on separate days to allow the radioisotope to decay thoroughly. Concentration images of the animals were normalized due to the lack of recorded tissue optical properties.

3. Results

3.1 Phantom validation

Fig. 2(a) displays the unmixed images for linearly increasing (top-to-bottom) amounts of Tb^{3+}-doped RLNPs on the left, and decreasing (top-to-bottom) Eu^{3+}-doped RLNPs on the right, at each concentration. The median values for each region of interest were plotted with respect to concentration. Fig. 2(b) shows the median raw signal detected from each nanophosphor concentration. Fig. 2(c) demonstrates this method's efficacy in separating the nanophosphors; the correlation between the samples was ($r = -0.98$).

#162598 - $15.00 USD Received 7 Feb 2012; revised 6 Apr 2012; accepted 7 Apr 2012; published 7 May 2012

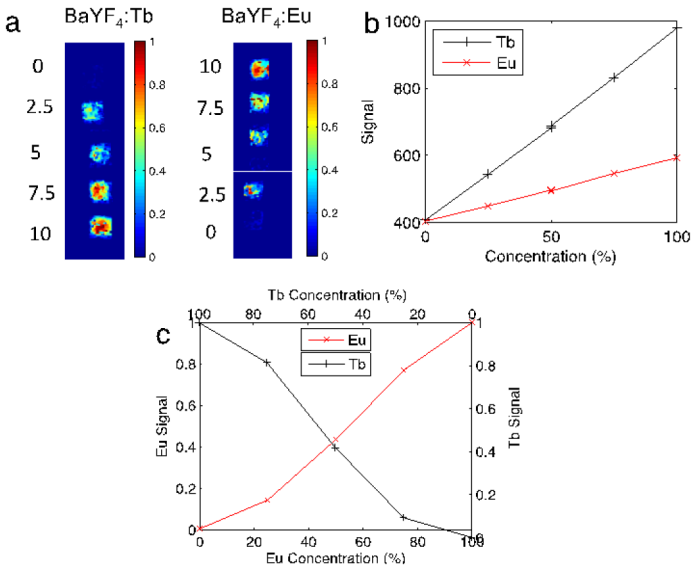

Fig. 2. (a) Shown are the $Ba_{0.55}Y_{0.3}F_2$:Tb^{3+} and $Ba_{0.55}Y_{0.3}F_2$:Eu^{3+} phosphor concentrations with increasing/decreasing concentration (top-to-bottom) of $Ba_{0.55}Y_{0.3}F_2$:Tb^{3+} / $Ba_{0.55}Y_{0.3}F_2$:Eu^{3+}, respectively. (b) The raw signal detected for each respective nanophosphor. (c) The relative median recovered concentration in each ROI plotted with respect to concentration.

3.2 Animal phantom validation

The locations of the subcutaneously injected RLNPs are shown in Fig. 3(a). The feasibility of this method in a pre-clinical subject with X-ray excitation is shown in Figs. 3(b)-3(d). Tb^{3+}-doped RLNPs embedded in the left and right flanks are shown successfully recovered in Fig. 3(b). The Eu^{3+}-doped RLNPs in the left foreleg and the right flank are shown successfully recovered in Fig. 3(c). As a control, inactive RLNPs in the right foreleg did not luminesce. Fig. 3(d) shows the results of the spectral unmixing algorithm, with the Eu^{3+}-doped RLNPs shown in red, and the Tb^{3+}-doped RLNP shown in green. The yellow in the multiplexed image indicates the presence of both types of nanophosphors.

The results of RLI with radiopharmaceutical excitation are shown in Fig. 4 (performed several days prior but on the same mouse as Fig. 3). The PET image of the four injected regions of ^{18}F with active and inactive particles is shown in Fig. 4(a); this image is included for spatial validation. All corners illuminate in the PET image because of the injection of ^{18}F with all particles. The unmixed Cerenkov image is shown in Fig. 4(b). Note the Cerenkov signal in each region, due to the injection of ^{18}F in each region; these correspond to the regions in the PET image. In particular, note the recovery of the Cerenkov light in the right foreleg, which contained the inactive control $Ba_{0.55}Y_{0.3}F_2$ nanocrystals along with ^{18}F. The successful recovery of Tb^{3+}-doped RLNPs and Eu^{3+}-doped RLNPs is demonstrated in Figs. 4(c)-4(d). The spectrally unmixed fused image is shown in Fig. 4(e), with Eu^{3+}-doped RLNPs in red, Tb^{3+}-doped RLNPs in green, and Cerenkov light in blue. Note that the doped nanoparticles did not emit in the control foreleg.

#162598 - $15.00 USD Received 7 Feb 2012; revised 6 Apr 2012; accepted 7 Apr 2012; published 7 May 2012

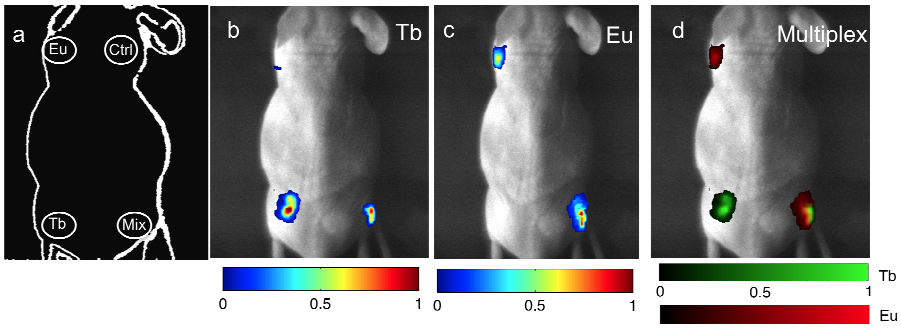

Fig. 3. X-ray Luminescence: (a) Schematic of the locations of each type of RLNP. The inactive particles are indicated with the abbreviation (Ctrl). (b,c) The unmixed signal from the $Ba_{0.55}Y_{0.3}F_2$:Tb and $Ba_{0.55}Y_{0.3}F_2$:Eu particles, respectively. (d) The unmixed multiplexed image with colorbars for the relative concentrations of $Ba_{0.55}Y_{0.3}F_2$:Tb and $Ba_{0.55}Y_{0.3}F_2$:Eu.

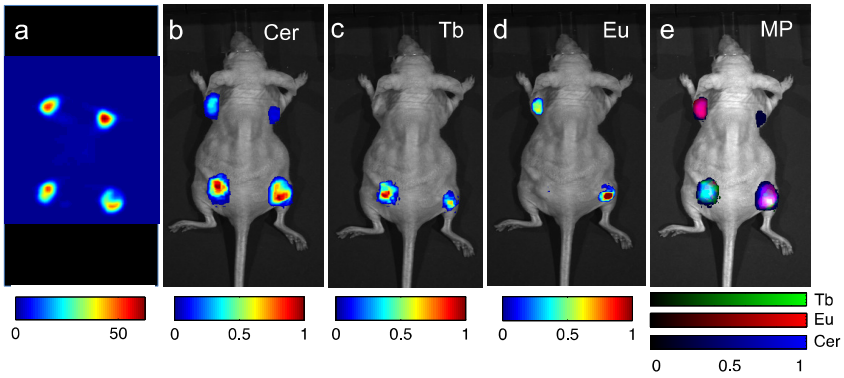

Fig. 4. Radiopharmaceutical luminescence: (a) Positron emission tomography image of the relevant RLNPs. (b) The unmixed signal from Cerenkov emission. (c,d) Unmixed signal from the $Ba_{0.55}Y_{0.3}F_2$:Tb^{3+} particles and $Ba_{0.55}Y_{0.3}F_2$:Eu^{3+}particles, respectively. (e) Unmixed multiplexed image with colorbars for the relative contributions of $Ba_{0.55}Y_{0.3}F_2$:Tb^{3+}, $Ba_{0.55}Y_{0.3}F_2$:Eu^{3+}, and Cerenkov emission.

4. Discussion and conclusions

The methods outlined in this paper demonstrate the ability of this particle system to simultaneously be used for multiple types of RLI; these may then be attached to distinct molecular targets. RLNPs may become an important analog to the current tools dedicated to pre-clinical imaging due to their great versatility. In one application, if injected with a radiopharmaceutical, the nanoparticles introduced in this study would enable multiple-targeting; this could prove to be an important method to identify the kinetics or accumulation after drug-injection. These RLNPs may also aid in the down-conversion of Cerenkov light emitted from the radiopharmaceutical [14–17]. In another application, these RLNPs may be used in conjunction with X-ray luminescence computed tomography [12] to recover high-resolution molecular-specific images. In yet another application, this RLNP system may aid in the on-line identification of response to radiation therapy. Through targeting of molecular markers specific for tumors, this method could provide feedback during therapy as to the status of treatment; the penetration of high-energy photons in conjunction with a light detector would ensure the ability to reach a larger depth in tissue.

In conclusion, we have demonstrated a nanoparticle platform for radioluminescence imaging which may be used to image multiple nanophosphors simultaneously using both radiopharmaceutical and X-ray irradiation. We showed an inverse relationship between

#162598 - $15.00 USD Received 7 Feb 2012; revised 6 Apr 2012; accepted 7 Apr 2012; published 7 May 2012

concentrations of the types of RLNPs, which showed successful separation of the contribution from the two emission signals. We then demonstrated this technology in a small-animal model.

Acknowledgments

The authors gratefully acknowledge the Department of Defense Breast Cancer Research Programs W81XWH-10-1-0506 (CMC), W81XWH-11-1-0087 (CS), and W81XWH-11-1-0070 (GP), the National Institutes of Health ICMIC P50CA114747, and the Center for Biomedical Imaging at Stanford-CBIS (CMC) for funding.

#162598 - $15.00 USD Received 7 Feb 2012; revised 6 Apr 2012; accepted 7 Apr 2012; published 7 May 2012